Journal of Alloys and Compounds 509 (2011) 3787–3794

Contents lists available at ScienceDirect

Journal of Alloys and Compounds

journal homepage: www.elsevier.com/locate/jallcom

The Al-rich region of the Al–Mn–Ni alloy system. Part I: Ternary phases at 750–950 °C

S. Balanetskyy[a,c,*], G. Meisterernst[b], M. Feuerbacher[a]

[a] Institut für Festkörperforschung, Forschungszentrum Jülich, D-52425 Jülich, Germany
[b] Crystallography Section, Ludwig-Maximilians-Universität München, D-80333 München, Germany
[c] I.N. Frantsevich Institute for Problems of Materials Science, 03680 Kiev 142, Ukraine

ARTICLE INFO

Article history:
Received 23 July 2010
Received in revised form 24 October 2010
Accepted 28 October 2010
Available online 10 November 2010

Keywords:
Intermetallics
Ternary alloy systems
Phase identification

ABSTRACT

Ternary phases in the Al-rich region of the Al–Mn–Ni alloy system were studied at 950, 850 and 750 °C. Two new ternary intermetallic compounds were revealed: the φ-phase (Al_5Co_2-type, *hP26*, $P6_3/mmc$: $a = 0.76632(16)$ and $c = 0.78296(15)$ nm) and the κ-phase (κ-$Al_{14.4}Cr_{3.4}Ni_{1.1}$-type, *hP227*, $P6_3/m$: $a = 1.7625(10)$ and $c = 1.2516(10)$ nm). The formation of the *O*-phase (*Pmmn*; *oP650*; *O*-$Al_{77}Cr_{14}Pd_9$-type; $a = 2.3316(16)$, $b = 1.2424(15)$ and $c = 3.2648(14)$ nm) was confirmed and its chemical composition as well as thermodynamic stability was specified.

1. Introduction

During the last two decades, Al-based alloy systems including transition metals attracted increased attention due to the multitude of binary and ternary intermetallics they often contain. In particular, structurally complex metallic alloys (CMAs) [1] and quasicrystals (QCs) are frequently found. Both these classes of materials constitute modern and very active fields in materials science. Various Al-based CMAs and QCs possess interesting physical and physicochemical properties which possess high potential for technological application (see for example Refs. [1–5] and references therein).

The formation of CMAs and QCs in the system Al–Mn–Ni was previously reported in the literature. In Ref. [6], during investigation of the phase equilibria in the Al-rich region of the Al–Mn–Ni alloy system (from 85 to 100 at.% Al) at 500, 600 and 630 °C, two ternary phases, $Al_{60}Mn_{11}Ni_4$ (termed X) and Y (indefinite composition and structure), were revealed. While the X-phase was identified to be thermodynamically stable, Y was identified as a metastable phase. The crystal structure of X-$Al_{60}Mn_{11}Ni_4$ was determined [7] (see crystallographic data in Table 1), using samples produced in Ref. [6]. Later on, this phase was termed *R*-phase, and we follow this nomenclature in our work. It should be mentioned that a metastable binary phase isostructural with ternary *R* was also found in the Al–Mn alloy system [8] (termed π-Al_4Mn in the original work).

In rapidly quenched $Al_{60}Mn_{11}Ni_4$, the observation of a nonperiodic phase was reported [9], which by Van Tendeloo et al. [10] was identified as the decagonal phase D_3 with periodicity ~1.24 nm (T_3 in original work). It was also established that the formation of D_3 does not require rapid quenching from the melt—the decagonal phase was also obtained in that work in slowly solidified alloys [10]. Annealing of the alloys containing the D_3-phase for 100 h at 400 °C was reported to lead to decomposition into two crystalline phases, $C_{3,I}$ (the *O*-phase in the present study) and $C_{3,II}$ (see Table 1). Their thermodynamic stability was not specified in the original work.

Singh and Ranganathan [11] reported results differing from those in Ref. [10]. These authors rapidly quenched an $Al_{60}Mn_{11}Ni_4$ alloy and subsequently annealed for 2 h at 600 °C. They found two different crystalline phases as decomposition products of D_3. One of them, termed *T*-phase in Ref. [11], was identified as body-centred orthorhombic (see Table 1), while the structure of the second crystalline phase was not specified.

Zhou et al. [12] found that in rapidly quenched $Al_{80}Mn_{10}Ni_{10}$ melts, a metastable decagonal phase coexists with the ternary hexagonal phase $Al_4Mn_{0.5}Ni_{0.5}$ (see Table 1). During subsequent annealing at 300 °C, it was found to decompose into orthorhombic phases similar to those found in Ref. [10].

All compounds mentioned in this brief literature survey are listed in Table 1. They are all CMAs according to the definition given in Ref. [1]. They have relatively large lattice constants and their unit cell contains more than a hundred atoms. The crystal structure of all these phases except $Al_4Mn_{0.5}Ni_{0.5}$, is based on pentagonal columnar atomic clusters of ~1.24 nm length composed from Mackay clusters [13,14].

* Corresponding author at: Maxim-Gorki-Str. 12, 09599-Freiberg, Germany. Tel.: +49 03731 259268.
E-mail address: dr.balanetskyy@alice-dsl.net (S. Balanetskyy).

0925-8388/$ – see front matter © 2010 Elsevier B.V. All rights reserved.
doi:10.1016/j.jallcom.2010.10.185

Table 1
Literature crystallographic data for the Al-rich ternary phases of Al–Mn–Ni.

Designation of phase		Space group	Pearson symbol	Structure type	Lattice periods (nm)			Alloy composition	Ref.
This work	Other				*a*	*b*	*c*		
R	X $Al_{60}Mn_{11}Ni_4$	*Bbmm*	oC156	$Al_{31}Mn_6Ni_2$	2.380	1.250	0.755	$Al_{80.15}Mn_{14.55}Ni_{5.30}$[a]	[7]
O	$C_{3,I}$	–	–	–	2.40	1.24	3.27	$Al_{60}Mn_{11}Ni_4$	[10]
–	$C_{3,II}$[b]	–	–	–	1.31	1.24	2.66	$Al_{60}Mn_{11}Ni_4$	[10]
D_3	T_3	Decagonal			–	1.24	–	$Al_{80.0}Mn_{10}Ni_{10}$	[9–12]
–	*T*	*I*-centred	–	–	1.24	1.26	3.14	$Al_{80.0}Mn_{14.7}Ni_{5.3}$	[11]
–	$Al_4Mn_{0.5}Ni_{0.5}$	*P*, hexagonal	–	–	1.272	–	1.261	$Al_{80}Mn_{10}Ni_{10}$[a]	[12]

[a] Phase composition.
[b] May also be represented in related monoclinic system [10].

In this paper, we report on results of a detailed investigation of the ternary phases in the Al–Mn–Ni alloy system in the Al-rich region ranging from 60 to 100 at.% Al in the temperature range from 750 to 950 °C. We address discrepancies revealed in previous works [6,7,10–12].

2. Experimental procedure

Alloys were produced from the constituent elements by levitation induction melting in a water-cooled copper crucible under Ar atmosphere. The purity of Al was 99.999%, of Mn 99.99%, and of Ni 99.99%. The weight of the ingots was typically about 5 g. Parts of the samples were annealed under an Ar atmosphere or vacuum for up to 958 h and subsequently water-quenched. The samples were investigated by scanning electron microscopy (SEM) and the phase compositions were measured by energy-dispersive X-ray analysis (EDX) in SEM. The composition of selected samples was determined by inductively coupled plasma optical emission spectroscopy. These analyses were used for calibrating the EDX measurements. The samples were further studied by selected area electron diffraction (SAED) in a JEOL 4000FX transmission electron microscope (TEM) operated at 400 kV. The TEM samples were powders spread on Cu grids covered by carbon films or thinned by mechanical grinding and subsequent ion-beam milling. Powder X-ray diffraction (PXRD) was carried out on a STOE diffractometer in transmission mode. We used Mo $K_{\alpha 1}$ radiation and a position-sensitive detector. Patterns were taken between $4^\circ \le 2\Theta \le 54^\circ$ with a step width of $\Delta 2\Theta = 0.02^\circ$. Differential thermal analysis (DTA) of selected samples was carried out with heating and cooling rates of 2–10 K/min.

3. Results and discussion

3.1. General information on phases in Al-rich region of Al–Mn–Ni between 950 and 750 °C

Fig. 1 is a schematic representation of the projected compositional ranges of the equilibrium phases between 950 and 750 °C. The sample preparation conditions and the results of microstructural and chemical analyses of the alloys containing the φ-, κ- and *O*-phases are shown in Table 2. Besides the ternary φ-, κ-, and *O*-phases, the neighbouring binaries in the Al–Mn and Al–Ni systems are also included (see crystallographic data e.g. in Refs. [15,16]). The binaries μ-Al_4Mn, $Al_{11}Mn_4$, and γ_2-Al_8Mn_5 dissolve small amounts of Ni, δ-Al_3Ni_2 and Al_3Ni dissolve small amounts of Mn. In the lower part of Fig. 1, the congruent β-AlNi phase (B2-structure) and γ-AlMn of the W-type (A2-structure) form a continuous range (β), since the B2 ↔ A2 transformation in the Al-rich region of Al–Mn–Ni takes place via a second-order phase transition [17]. Since γ-AlMn is a high-temperature phase [18], below 840 °C the β-range separates from binary Al–Mn and the β-phase may be considered as a solid solution of Mn in binary β-AlNi.

Besides the binary phases and their ternary solid solutions above, three ternary phases were found in the present study. These phases were observed in as-cast samples as well as in samples annealed up to 958 h (see Table 2) and are hence concluded to be thermodynamically stable phases in the Al–Mn–Ni alloy system. Two of these phases, the hexagonal φ- and κ-phases (see Fig. 1 and Table 2), are revealed in the Al–Mn–Ni alloy system for the first time. The orthorhombic *O*-phase was reported earlier [10] (termed $C_{3,I}$-phase in that work, Table 1), but its thermodynamic stability was not specified. The other periodic ternary phases listed in Table 1, were not found in the present study. Small amounts of the metastable decagonal D_3-phase were observed by TEM in as-cast alloys of composition close to that of the *O*-phase, but this phase transforms quickly to distorted or twinned *O*-phase under the electron beam, which is in agreement with the findings in Ref. [10].

3.2. The ternary hexagonal φ-, κ- and related phases

In Al–Mn–Ni, the ternary hexagonal φ-phase (SAED and PXRD patterns in Figs. 2a–c and 3a, respectively) is formed incongruently by the peritectic reaction:

$$L + \gamma_1 + T \leftrightarrow \varphi$$

at about 993 °C. The initial composition of φ at the temperature of peritectic reaction is estimated as about $Al_{71.4}Mn_{23.2}Ni_{5.4}$ (Fig. 1) according to SEM-EDX analysis of the corresponding as-cast and sub-solidus annealed alloys.

Refinement of the PXRD data of the φ-phase (Table 3) resulted in lattice parameters $a = 0.76632(16)$ and $c = 0.78296(15)$ nm for the $Al_{73.1}Mn_{19.1}Ni_{7.8}$ composition (no. 10 in Table 2). The PXRD pattern was also calculated using the structural model of the metastable binary φ-$Al_{10}Mn_3$ from Ref. [19].

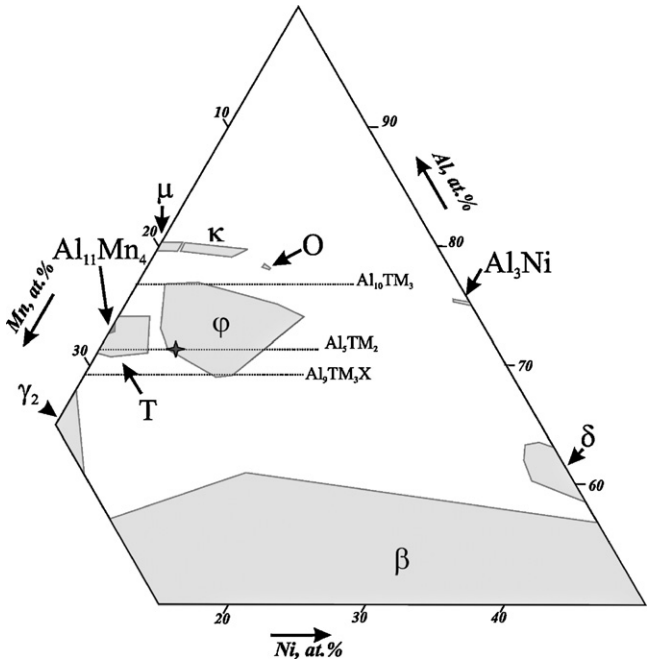

Fig. 1. Scheme of the projected compositional ranges of the Al-rich Al–Mn–Ni phases between 950 and 750 °C. The peritectic composition of the φ-phase is marked by a star. TM stands for transition metals, X for vacancies in the Al- or TM substructure. The stoichiometry of related binary intermetallics is shown by dotted lines.

Table 2
Metallurgical characteristics of Al–Mn–Ni alloys containing the φ-, κ- and *O*-phases.

No.	Composition of alloy (at.%)			Heat treatment (°C/h)	Phase	Phase composition (at.%)		
	Al	Mn	Ni			Al	Mn	Ni
1	73.2	19.0	7.8	950/118	φ	73.2	19.0	7.8
2	70.6	25.4	4.0	950/118	φ	71.5	23.5	5.0
					T	71.2	25.2	3.6
					γ_2	65.5	33.5	1.0
3	67.5	21.1	11.4	950/118	φ	69.2	21.3	9.5
					γ_2	62.7	34.5	2.8
					β	56.5	19.0	24.5
4	70.4	10.4	19.2	950/118	φ	72.5	15.3	12.2
					δ	62.0	2.5	35.5
					L	~80.0	~4.5	~5.5
5	75.6	21.2	3.2	950/118	φ	74.3	22.2	3.5
					L	~81.5	~17.5	~1.0
6	79.0	20.0	1.0	850/139	φ	77.0	20.8	2.2
					μ	79.6	19.9	0.5
7	78.2	19.6	2.2	850/135	φ	77.0	20.2	2.8
					κ	79.6	18.9	1.5
8	81.7	16.1	2.2	850/118	κ	80.3	17.5	2.2
					L	~90.0	~8.0	~2.0
9	72.5	26.3	1.2	850/139	φ	73.0	23.0	4.0
					T	71.6	27.6	0.8
					($Al_{11}Mn_4$)	72.7	26.8	0.5
10	73.1	19.1	7.8	850/135	φ	73.1	19.1	7.8
11	78.1	5.9	16.0	850/139	φ	74.0	12.5	13.5
					δ	63.3	0.6	36.1
					L	~84.0	~3.5	~12.5
12	67.7	20.9	11.4	850/167	φ	69.3	19.9	10.8
					γ_2	63.0	33.9	3.1
					β	57.7	14.3	28.0
13	79.1	18.8	2.1	750/161	φ	77.0	20.1	2.9
					κ	79.6	18.1	2.3
					μ	79.6	19.1	1.4
14	77.4	14.4	8.2	750/161	φ	75.3	14.8	9.9
					κ	79.2	15.2	5.6
					O	78.6	13.2	8.2
15	78.8	13.4	7.8	750/958	κ	79.9	13.7	6.4
					O	78.6	12.8	8.6
16	76.9	12.1	11.0	750/958	φ	75.0	14.1	10.9
					O	78.0	13.1	8.9
					(Al_3Ni)	75.3	1.2	23.5
17	73.4	19.2	7.4	750/161	φ	73.4	19.2	7.4
18	67.6	21.1	11.3	750/958	φ	69.4	21.2	9.4
					β	61.5	22.1	16.4

L, solidified liquid.

Obviously, the ternary φ-phase reported in the present paper can be understood as a Ni-stabilized variant of the metastable binary φ-phase reported earlier in Refs. [19,20]. Similar stabilization effects by Si have been reported: the ternary stable Al_9Mn_3Si-phase (β-AlMnSi) is also of Al_5Co_2-type [21]. Further Al_5Co_2-type phases are known not only in the Al-based alloy systems (Al–Co, Al–Mn, Al–Rh, Al–Mn–Ni, Al–Mn–Si, Al–Fe–Ni, etc.), but also in numerous alloy systems of TM metals with *p*-elements [22]. The crystal structure of φ-$Al_{10}Mn_3$ is similar to that of Al_5Co_2 but has two unoccupied atomic sites corresponding to the 2(*d*) positions [19,23], i.e. compared with Al_5Co_2, in the structure of φ-$Al_{10}Mn_3$ two atomic vacancies exist in the transition metal (TM) substructure. Therefore its unit cell contains 26 atoms instead of 28 atoms as that of Al_5Co_2.

In this view, it is worthwhile to discuss the compositional range of ternary φ-AlMnNi (see Part II of this paper [24]). The composition of φ-AlMnNi at the peritectic point corresponds well to the Al_5TM_2 stoichiometry (Fig. 1). The most Al-rich extension corresponds to $Al_{10}TM_3$. The expansion of the homogeneity region of φ-AlMnNi from the peritectic composition $Al_{71.4}Mn_{23.2}Ni_{5.4}$ with decreasing of temperature from 993 to 850 °C may be accompanied by the formation of vacancies in the TM-substructure of Al_5Co_2-type structure during replacement of Ni by Mn and by replacement of Mn by Ni (see scheme in Fig. 1). The most Al-poor region of φ-AlMnNi formally corresponds to the stoichiometry Al_9TM_3X, like in the case of β-Al_9Mn_3Si, where X is Si. The replacement of Mn by Ni in this case may be accompanied by the formation of vacancies in the Al-substructure of the Al_5Co_2-type structure. Surely, this qualitative assessment requires quantitative confirmation. Therefore the determination of the atomic structure of φ-AlMnNi for different compositions is necessary.

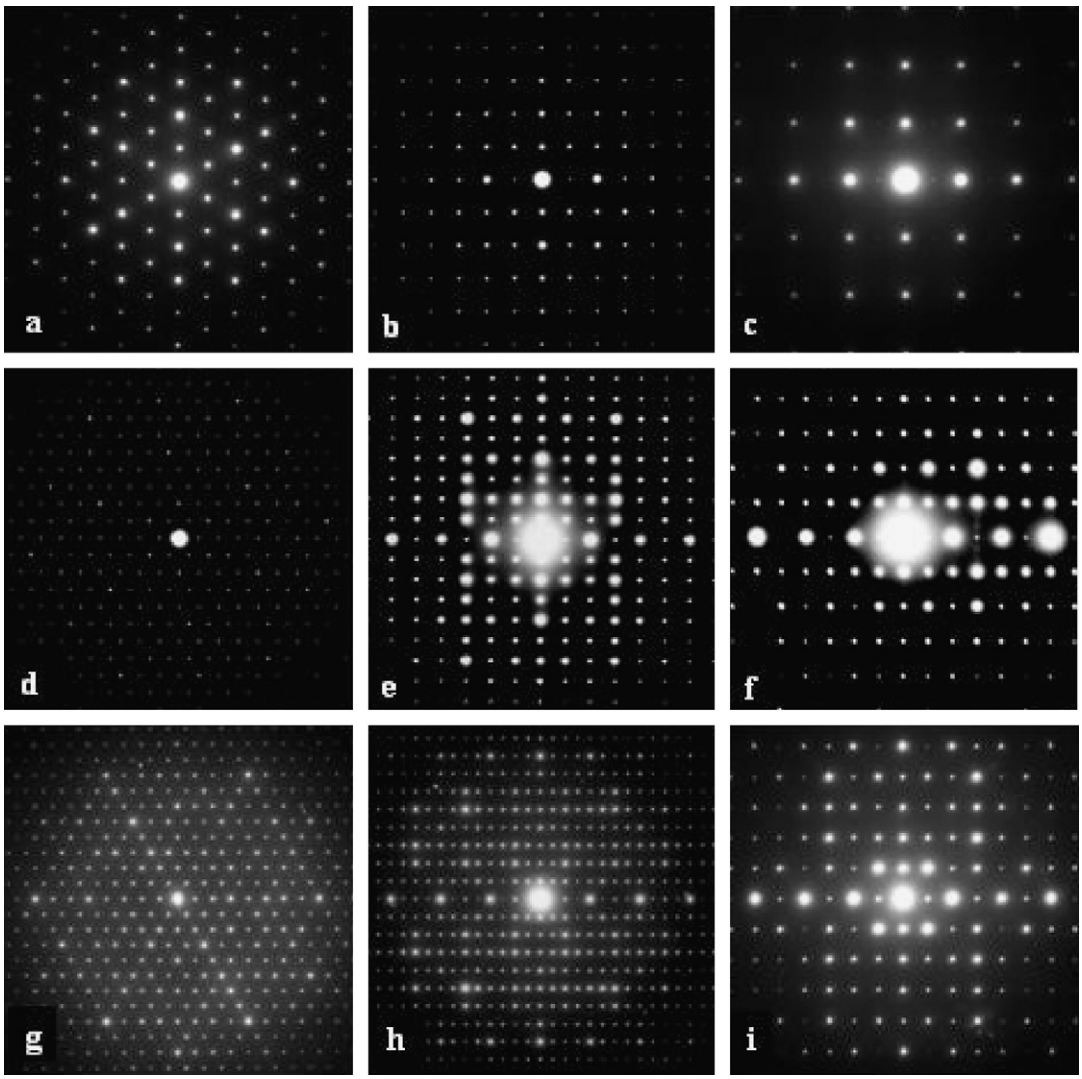

Fig. 2. SAED patterns of the φ-phase along zone axes [0 0 0 1] (a), [1 0 $\bar{1}$ 0] (b), and [$\bar{1}$ 1 0 0] (c). Of the κ-phase along [0 0 0 1] (d), [1 0 $\bar{1}$ 0] (e), and [$\bar{1}$ 1 0 0] (f). Of the μ-phase along [0 0 0 1] (g), [1 0 $\bar{1}$ 0] (h), and [$\bar{1}$ 1 0 0] (i).

Table 3
PXRD data of the φ-phase of $Al_{73.1}Mn_{19.1}Ni_{7.8}$ composition. The intensities are calculated according to the atomic parameters given in Ref. [19].

No.	*H*	*K*	*L*	d_{obs}	d_{calc}	I/I_{0obs}	I/I_{0calc}
1	1	0	0	0.66383	0.66365	29.0	80.5
2	1	0	1	0.50600	0.50626	3.2	9.7
3	0	0	2	0.39161	0.39148	27.0	17.5
4	2	0	0	0.33199	0.33183	8.0	4.3
5	2	0	1	0.30560	0.30552	39.8	15.9
6	1	0	3	0.24286	0.24288	9.7	32.2
7	3	0	0	0.22125	0.22122	9.9	24.0
8	3	0	1	0.21283	0.21288	83.2	100.0
9	2	1	2	0.21121	0.21120	100.0	85.0
10	2	0	3	0.20513	0.20514	77.8	62.0
11	0	0	4	0.19571	0.19574	19.7	15.1
12	1	0	4	0.18778	0.18774	3.7	6.9
13	3	1	1	0.17921	0.17918	13.6	5.2
14	3	0	3	0.16876	0.16875	8.1	7.2
15	2	1	4	0.15430	0.15431	4.6	2.7
16	4	0	2	0.15273	0.15276	2.9	2.3
17	1	0	5	0.15239	0.15241	3.0	0.1
18	3	1	3	0.15045	0.15042	6.7	2.4
19	3	0	4	0.14647	0.14659	1.1	3.5
20	4	1	0	0.14482	0.14482	1.5	0.2

The ternary hexagonal κ-phase (SAED and PXRD patterns in Figs. 2d–f and 3b, respectively) in the Al–Mn–Ni alloy system is formed incongruently by the peritectic reaction:

$$L + \varphi + \mu \leftrightarrow \kappa$$

at about 867 °C. The initial composition of κ at the temperature of the peritectic reaction is estimated as be about $Al_{80.0}Mn_{18.5}Ni_{1.5}$.

As in the case of the φ-phase, the extension and location of the homogeneity region in the alloy system depend on temperature. In the projection in scheme in Fig. 1, one can see that the κ-phase has practically the same Al content as μ-Al_4Mn, i.e. about 80 at.%, but some Mn is replaced by Ni. The increase of Ni-content in κ is accompanied by a small decrease of Al-content.

The PXRD pattern of the κ-phase (Table 4) was indexed using lattice parameters $a = 1.7625(10)$ and $c = 1.2516(10)$ nm for the $Al_{80.3}Mn_{17.5}Ni_{2.2}$ composition. We also calculated a PXRD pattern using the structure model presented in Ref. [25], in which the Cr atoms were replaced by Mn.

Phases isostructural with κ-Al–Mn–Ni are known in the Al–Cr–Ni [25,26] and Al–Cr–Cu (ξ-Al–Cr–Cu) [27,28] alloy systems. While in Al–Cr–Ni it is known only at a single composition of about $Al_{76}Cr_{18}Ni_6$ [25,26], in Al–Cr–Cu it occupies a relatively large compositional region [28].

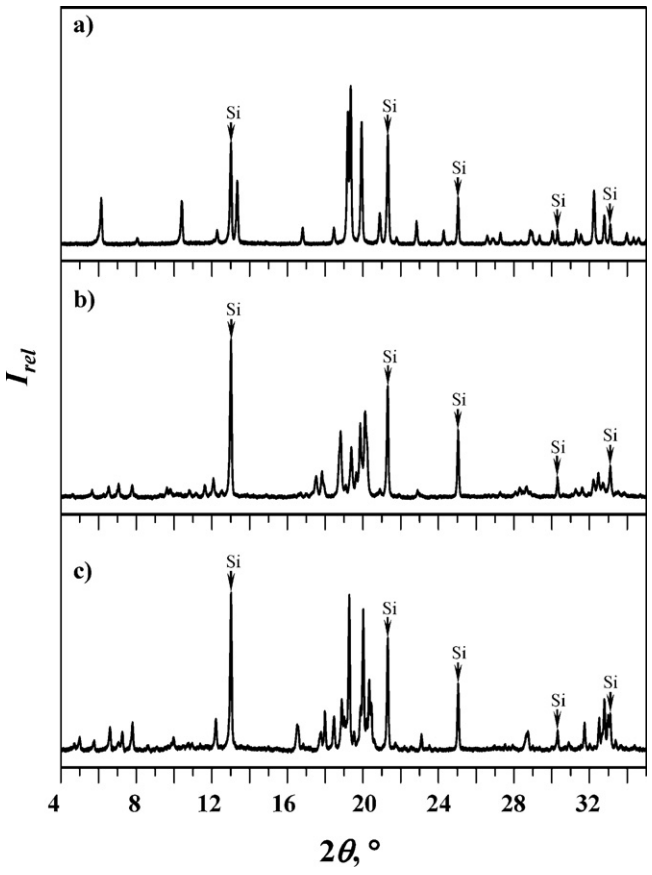

Fig. 3. PXRD patterns (Mo Kα) of the φ-phase (a), the κ-phase (b), and of μ-Al_4Mn (c). The composition of the phases and indexing are listed in Tables 3–5. Reflections which belong to Si, which was used as internal standard, are correspondingly labelled.

Table 4
PXRD data of the κ-phase of $Al_{80.3}Mn_{17.5}Ni_{2.2}$. The intensities are calculated according to the atomic parameters given in Ref. [25].

No.	*H*	*K*	*L*	d_{obs}	d_{calc}	I/I_{0obs}	I/I_{0calc}
1	1	1	0	0.88346	0.88125	2.5	34.0
2	1	1	1	0.72092	0.72055	6.7	9.8
3	2	0	1	0.65159	0.65160	2.8	4.1
4	0	0	2	0.62383	0.62579	11.5	4.1
5	2	1	0	0.57739	0.57691	14.2	25.3
6	2	1	1	0.52396	0.52393	13.1	12.6
7	2	2	0	0.44111	0.44062	2.5	2.0
8	2	1	2	0.42370	0.42417	10.0	16.7
9	2	2	1	0.41562	0.41562	7.3	6.9
10	3	1	1	0.40104	0.40102	3.4	3.8
11	1	1	3	0.37701	0.37707	7.3	5.2
12	4	0	1	0.36497	0.36500	3.8	0.2
13	3	1	2	0.35055	0.35064	13.1	25.8
14	2	1	3	0.33755	0.33806	20.8	16.5
	3	2	1		0.33722		13.3
15	4	0	2	0.32541	0.32580	6.9	16.8
16	5	0	2	0.27424	0.27437	2.3	2.7
17	5	2	0	0.24435	0.24441	3.8	1.0
18	1	1	5	0.24038	0.24079	3.0	1.0
19	3	2	4	0.23314	0.23332	23.2	14.6
	6	1	0		0.23277		10.3
20	5	1	3	0.22905	0.22911	29.5	7.0
21	6	0	3	0.21717	0.21720	76.1	55.1
22	5	2	3	0.21083	0.21089	57.6	50.7
23	4	4	2	0.20802	0.20781	27.7	1.0
24	7	0	2	0.20587	0.20591	85.2	100.0
25	6	1	3	0.20319	0.20327	100.0	86.4

Table 5
PXRD data of the μ-phase of $Al_{79.8}Mn_{20.2}$. The intensities are calculated according to the atomic parameters given in Ref. [32].

No.	*H*	*K*	*L*	d_{obs}	d_{calc}	I/I_{0obs}	I/I_{0calc}
1	2	0	0	0.86461	0.86668	4.0	1.1
2	2	0	1	0.81585	0.81780	7.7	11.0
3	2	0	2	0.70909	0.70941	5.2	0.6
4	2	1	0	0.65279	0.65515	0.7	4.3
5	0	0	4	0.61707	0.61748	13.9	14.3
6	2	1	2	0.57809	0.57875	4.3	8.3
7	3	0	1	0.56164	0.56260	11.3	14.9
8	3	0	2	0.52273	0.52334	17.4	18.9
9	0	0	6	0.41391	0.41165	4.1	1.8
10	4	0	2	0.40858	0.40890	7.9	5.2
11	3	2	2	0.37888	0.37852	4.1	4.9
12	2	0	6	0.37210	0.37184	3.8	11.7
13	3	2	3	0.35806	0.35808	3.2	3.0
14	3	2	4	0.33380	0.33433	20.4	21.3
15	4	2	2	0.31752	0.31663	8.5	3.5
16	7	0	1	0.24698	0.24639	16.4	12.5
17	5	3	1	0.24630	0.24639	14.8	0.1
18	5	2	5	0.24241	0.24198	3.7	6.6
19	7	0	4	0.22983	0.22983	11.1	2.2
20	3	0	10	0.22703	0.22711	23.8	22.2
21	7	0	5	0.22125	0.22137	21.6	17.7
22	8	0	0	0.21638	0.21667	32.5	24.0
23	5	0	9	0.21495	0.21517	20.8	14.5
24	8	0	2	0.21343	0.21341	18.9	9.1
25	5	3	6	0.21200	0.21219	100.0	100.0
26	3	0	11	0.20923	0.20929	11.6	9.8
27	0	0	12	0.20568	0.20583	28.0	23.3
28	8	0	4	0.20424	0.20445	90.8	82.6

The φ- and κ-phases of Al–Mn–Ni are structurally closely related with the binary μ- (SAED and PXRD patterns in Figs. 2g–i and 3c, respectively) and λ-phases of Al–Mn [25,27,29–31]. The structure of all of these phases is based on icosahedral clusters grouped in more complex agglomerates, so-called I3-clusters [26,29].

The refinement of the PXRD data of the μ-phase (Table 5) yields the lattice parameters $a = 2.0015(21)$ and $c = 2.4699(17)$ nm for the composition $Al_{79.8}Mn_{20.2}$. The powder XRD pattern was also calculated using the structural model of μ given in Ref. [32].

In spite of the close structural relationship between the φ-, κ-, and μ-phases, their diffraction patterns (Figs. 2 and 3) are distinctly different. This gives a possibility to distinguish these phases by diffraction methods in samples were they are coexisting. Although the compositions of κ and μ differ only by about 1 at.% TM, they are also easily distinguishable in SEM (Fig. 4).

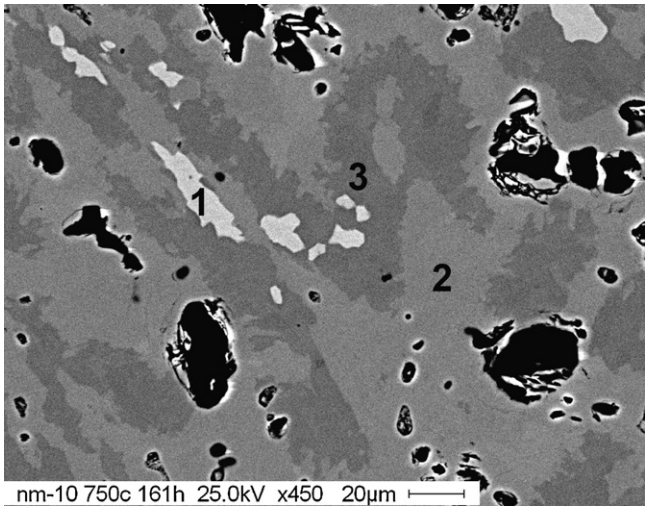

Fig. 4. SEM image of alloy no. 13 (Table 3). The grey-values correspond to the φ-phase (1), the κ-phase (2), and the μ-phase (3). Black contrast corresponds to pores in the ingot.

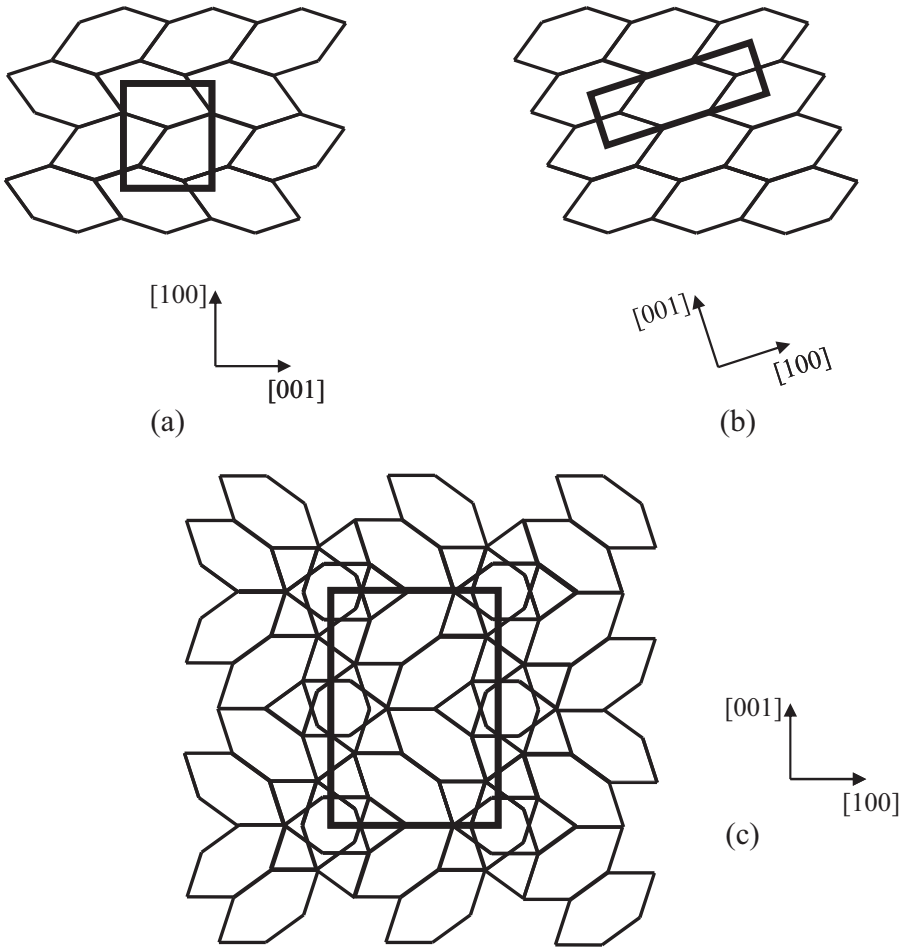

Fig. 5. Tiling models of [0 1 0] projections of the *T*-phase (a), the *R*-phase (b), and the *O*-phase (c).

Note that the comparison of the intensities of calculated and experimental PXRD spectra show a rather qualitative agreement (Tables 3–5). This holds for the φ-, κ-, and μ-phases and reflects the fact that for neither of these accurate structure models are available in the literature.

3.3. The ternary orthorhombic O-phase

As mentioned above, the *O*-phase in Al–Mn–Ni was reported earlier [10] (see Table 1), but its exact chemical composition and thermodynamic stability was not specified. In the present study, using as-cast and annealed samples, it could be established that the *O*-phase in Al–Mn–Ni is formed incongruently by the peritectic reaction:

$$L + \varphi + \kappa \leftrightarrow O$$

at about 757 °C. At 750 °C it occupies a small compositional region around $Al_{78.5}Mn_{13.0}Ni_{8.5}$.

Other phases similar to *O*-Al–Mn–Ni were revealed in the systems Al–Cr–Fe [33] (termed $C_{3,I}$ in the original work) and Al–Cr–Pd [14] (termed *O* in the original work. Worth noting, that in contrast to Ref. [14], the *O*-phase was not found in Ref. [34]). While the composition of $C_{3,I}$–Al–Cr–Fe was not determined in Ref. [33], the composition of *O*-$Al_{77}Cr_{14}Pd_9$, determined in Ref. [14], is very similar to that of the *O*-phase found in the present study if Cr is replaced by Mn and Pd by Ni. This is not surprising taking into account the position of these elements in the periodic table.

According to Refs. [13,14], the *O*-phase is structurally closely related to binary *T*-Al_3Mn and the ternary *R*-phase (Table 1). All these structures are based on pentagonal columnar clusters of about 1.24 nm length. Connecting the centres of neighbouring clusters, the structure of *T* can be described using an alternating arrangement of elongated hexagons (EH), while the structure of *R* can be described by their parallel arrangement (Fig. 5). In a similar way, the structure of *O* can be described using an alternating arrangement of coupled EH in combination with pentagonal stars (Fig. 5). The latter are composed by five superposed EHs. The lattice parameters of the *T*-, *R*- and *O*-phases are related as

$$a_O \approx \tau a_T \approx a_R$$

$$b_O \approx b_T \approx b_R$$

$$c_O \approx (1+\tau)c_T \approx \tau(1+\tau)c_R$$

where *a*, *b*, and *c* are the lattice parameters of the corresponding phases and τ is the number of the golden mean 1.6180.

SAED and PXRD patterns of the *O*-phase are shown in Figs. 6 and 7, respectively. The PXRD pattern of the *O*-phase (Table 6) was indexed using the lattice parameters $a = 2.3316(16)$, $b = 1.2424(15)$, and $c = 3.2648(14)$ nm for the $Al_{78.4}Mn_{13.3}Ni_{8.3}$ composition. Unfortunately, a quantitative atomic model for the *O*-phase is not available in the literature. The models published [14,35] are qualitative models on the basis of cluster-decorated tillings, which are inapplicable for the calculation of PXRD reflection intensities.

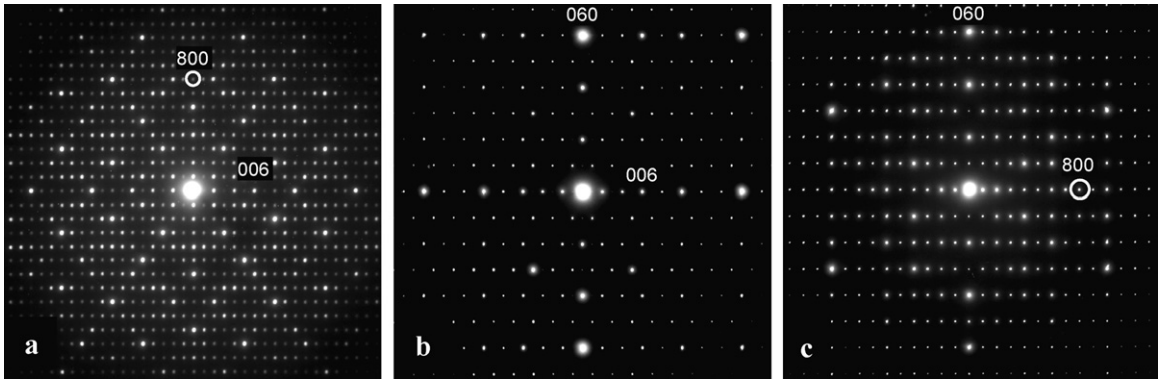

Fig. 6. SAED patterns of the *O*-phase along zone axis [0 1 0] (a), [1 0 0] (b), and [0 0 1] (c).

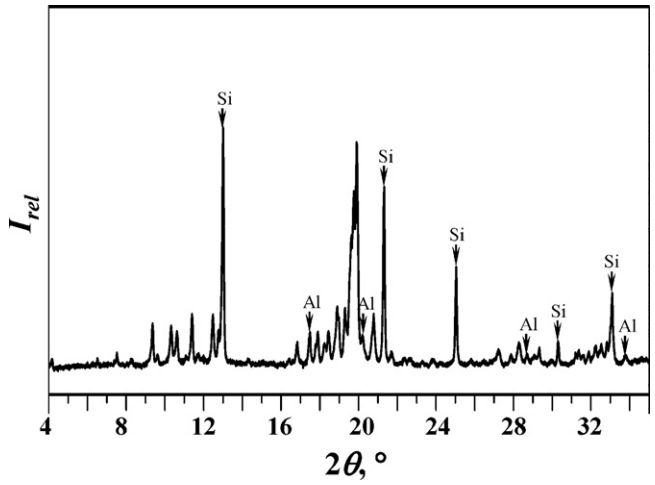

Fig. 7. PXRD patterns of the *O*-phase. The composition of the phase and indexing are listed in Table 6. Reflections which belong to Si (which was used as internal standard), and those which belong to (Al) are labelled correspondingly.

Table 6
PXRD data of the *O*-phase of $Al_{78.4}Mn_{13.3}Ni_{8.3}$.

No.	*H*	*K*	*L*	d_{obs}	d_{calc}	I/I_{0obs}
1	0	1	2	0.98731	0.98864	2.1
2	1	0	5	0.62888	0.62876	2.1
3	0	0	6	0.54431	0.54413	4.3
4	0	2	4	0.49473	0.49432	1.7
5	0	1	7	0.43702	0.43664	18.0
6	4	2	0	0.42495	0.42507	4.2
7	4	2	3	0.39615	0.39594	17.0
8	6	0	1	0.38496	0.38588	14.2
9	0	3	4	0.36876	0.36932	3.6
10	1	0	9	0.35866	0.35844	22.6
11	0	3	5	0.34895	0.34973	4.5
12	6	2	1	0.32765	0.32779	22.1
13	7	1	1	0.32020	0.32018	15.3
14	5	0	9	0.28580	0.28632	2.2
15	0	2	12	0.24908	0.24921	2.3
16	3	3	10	0.24310	0.24348	8.9
17	8	3	4	0.22864	0.22879	14.4
18	9	2	5	0.22422	0.22453	9.2
19	2	5	6	0.22186	0.22190	14.9
20	1	0	15	0.21652	0.21671	24.5
21	8	3	7	0.21211	0.21224	24.9
22	2	5	8	0.20857	0.20880	57.0
23	11	1	2	0.20726	0.20726	76.4
24	1	6	1	0.20567	0.20585	100.0
25	6	1	14	0.19714	0.19742	21.7

While we found the *O*-phase in as-cast as well as samples annealed up to 958 h (Table 2), the *R*-phase, reported earlier in Refs. [6,7], was not found. Therefore we cannot confirm the formation of a thermodynamically stable *R*-phase in Al–Mn–Ni. The composition $\sim Al_{80}Mn_{15}Ni_6$ reported in Refs. [6,7] for the *R*-phase corresponds, according to our data, to the hexagonal κ-phase.

Acknowledgements

We thank C. Thomas, M. Schmidt, and E.-M. Würtz for technical contributions and M. Heggen, S. Mi, B. Grushko and T.Ya. Velikanova for helpful discussions. This work was financially supported by the DFG (project Ur51/8-2) and the 6th Framework EU Network of Excellence "Complex Metallic Alloys" (Contract No. NMP3-CT-2005-500140).

References

[1] K. Urban, M. Feuerbacher, J. Non-Cryst. Solids 334, 335 (2004) 143.
[2] M. Feuerbacher, Acta Mater. 53 (2005) 3833.
[3] M. Krajči, J. Hafner, Phys. Rev. B68 (2003) 165202.
[4] M. Heggen, L. Houben, M. Feuerbacher, Nat. Mater. 9 (2010) 332.
[5] J. Dolinsek, M. Feuerbacher, M. Jagodic, Z. Jaglicic, M. Heggen, K. Urban, J. Appl. Phys. 106 (2009) 043917.
[6] G.V. Raynor, J. Inst. Met. 70 (1944) 507.
[7] K. Robinson, Acta Crystallogr. 7 (1954) 494.
[8] X.Z. Li, K.H. Kuo, Philos. Mag. B65 (1992) 525.
[9] G.V.S. Sastry, C. Suryanarayana, M. Van Sade, G. Van Tendeloo, Mater. Res. Bull. 13 (1978) 1065.
[10] G. Van Tendeloo, J. Van Landuyt, S. Amelinckx, S. Ranganathan, J. Microsc. 149 (1988) 1.
[11] A. Singh, S. Ranganathan, Mater. Sci. Eng. A181–A182 (1994) 754.
[12] W.L. Zhou, X.Z. Li, K.H. Kuo, Scripta Metall. 23 (1989) 1571.
[13] X.Z. Li, K. Hiraga, Sci. Rep. RITU A42 (1996) 213.
[14] W. Sun, K. Yubuta, K. Hiraga, Philos. Mag. B71 (1995) 71.
[15] O. Dovbenko, T. Velikanova, S. Balanetskyy, Landolt-Börstein, IV/11A3, 2005, pp. 215–252.
[16] P. Villars, L.D Calvert (Eds.), Pearson's Handbook of Crystallographic Data for Intermetallic Phases, vol. 1, 2nd ed., 1991, p. 948.
[17] R. Kainuma, M. Ise, K. Ishikawa, I. Ohnuma, K. Ishida, J. Alloy Compd. 269 (1998) 173.
[18] T.B. Massalski (Ed.), Binary Alloy Phase Diagrams, vol. 2, 2., Materials-Park, OH, ASM International, 1990, p. 970.
[19] M.A. Taylor, Acta Crystallogr. 12 (1959) 393.
[20] J.L. Murray, A.J. McAlister, R.J. Schaffer, L.A. Bendersky, F.S. Biancaniello, D.L. Moffat, Metall. Trans. 18A (1986) 385.
[21] K. Robinson, Acta Crystallogr. 5 (1952) 397.
[22] A. Harsta, S. Rundquist, J. Solid State Chem. 70 (1987) 210.
[23] J.B. Newkirk, P.J. Black, A. Damjanovic, Acta Crystallogr. 14 (1961) 532.
[24] S. Balanetskyy, G. Meisterernst, M. Feuerbacher, J. Alloy Compd., in press.
[25] R.E. Marsh, Acta Crystallogr. B54 (1998) 925.
[26] X.Z. Li, K. Hiraga, A. Yamamoto, Philos. Mag. A76 (1997) 657.
[27] K. Sugiyama, H. Saito, K. Hiraga, J. Alloy Compd. 342 (2002) 148.
[28] B. Grushko, E. Kowalska-Strzęciwilk, B. Przepiórzyński, M. Surowiec, J. Alloy Compd. 417 (2006) 121.
[29] G. Kreiner, H.F. Franzen, J. Alloy Compd. 221 (1995) 15.
[30] M. Uchida, Y. Matsui, Philos. Mag. 81 (2001) 2121.
[31] S. Ranganathan, A. Singh, A.P. Tsai, Philos. Mag. Lett. 82 (2002) 13.

[32] C.B. Shoemaker, D.A. Keszler, D. Shoemaker, Acta Crystallogr. B45 (1989) 13.
[33] V. Demange, J.S. Wu, V. Brien, F. Machizaud, J.M. Dubois, Mater. Sci. Eng. 294 (2000) 79.
[34] W. Kowalski, B. Grushko, D. Pavlyuchkov, M. Surowiec, J. Alloy Compd. 496 (2010) 129.
[35] H.X. Sui, K. Sun, K.H. Kuo, Philos. Mag. A75 (1997) 379.